Lidar-based snow monitoring: cable car deployment in the Austrian Alps

Berin DIKIC,[1] Thomas GOELLES,[1,2] Christoph GAISBERGER,[2] Birgit SCHLAGER,[1,2] Stefan MUCKENHUBER,[1,2,3] Pedro BATISTA,[4] Markus KEUSCHNIG,[5] Markus SCHRATTER[1]

[1] *Electrics/Electronics & Software, Virtual Vehicle Research GmbH, Graz, Austria*
[2] *Institute of Geography and Regional Science, University of Graz, Graz, Austria*
[3] *Institute of Industrial Management, FH JOANNEUM, Austria*
[4] *Institute for Systems and Robotics, Instituto Superior Técnico, Universidade de Lisboa, Lisbon, Portugal*
[5] *GEORESEARCH Forschungsgesellschaft mbH, Puch bei Hallein, Austria*
Correspondence: Thomas Goelles <thomas.goelles@uni-graz.at>, Berin Dikic <berin.dikic@v2c2.at>

ABSTRACT.

Traditional methods for surveying the spatial and temporal distribution of snow are often time-consuming, costly, and potentially hazardous. To address these challenges, we propose a novel approach utilizing a newly developed sensor system based on cost-effective industrial lidar sensors. This system is designed to be mounted on cable cars, enabling continuous environmental scanning during regular operations. The system integrates data from the lidar, an Inertial Measurement Unit (IMU), and Global Navigation Satellite System (GNSS), employing a Simultaneous Localization And Mapping (SLAM) algorithm to generate detailed maps of the area. In our initial testing on Hoher Sonnblick, we benchmarked our data against conventional laser scanning and structure-from-motion techniques. Four experimental runs were conducted over a single day using the same cable car equipped with our setup. The SLAM algorithm had some difficulties in areas without many distinct features and aligning two 3D point clouds without Ground Control Points (GCPs) was challenging. However, our system achieved precision within the centimeter range, with the error mean of -0.0002m **and the standard deviation of** 0.0328m**, enabling us to accurately detect day to day changes. Despite some operational challenges, the results confirm the feasibility and effectiveness of this innovative method.**

INTRODUCTION

Understanding the spatial characteristics of a snowpack in mountainous regions, particularly parameters like Snow Water Equivalent (SWE), is crucial for several critical aspects, including the assessment and forecasting of snow-free periods, estimation of snow-melt volume, and evaluation of avalanche hazards (e.g., Deems and others, 2013). This knowledge is relevant for climatological studies (Marty, 2013), tourism (e.g., Robert and others, 2019), hydro-power, water supply (Beniston and others, 2018), and ecological aspects (Rixen and others, 2022). The intricate interplay between snowfall, wind, terrain, and vegetation, compounded by the process of snow metamorphism, presents a challenge for accurate measurement of the snowpack. Manual assessment of snow depth is not only costly, time-intensive, and potentially hazardous but also disrupts the snowpack. Automatic snow depth monitoring, in conjunction with an automatic weather station, does not have these disadvantages, but to this point is still mostly point observation based. Furthermore, relying solely on point measurements proves inadequate in capturing the variability inherent in snow depth across diverse terrains (Bühler and others, 2015).

Light Detection and Ranging (lidar) is able to acquire high-resolution data, ranging from a few millimeters to a few dozen millimeters between adjacent points, depending on the range (e.g., Pesci and others, 2011). This point data is typically acquired from the ground using Terrestrial Laser Scanners (TLSs) or from the air using Unmanned Aircraft System (UAS) or common aircrafts. Calculating snow depth requires two co-registered point clouds, by subtracting a dataset without snow from one with snow. Therefore, to study the temporal evolution of the snow cover, one dataset without snow is sufficient, while the current snow

cover needs to be monitored at the desired time intervals. In recent years, semi-permanent installations of TLSs to monitor glaciers have been erected (Voordendag and others, 2022, 2023), but they come at a high cost since a housing with power supply needs to be built or adapted, and the TLSs cost more than € 150,000. An alternative to a static, long-range mounted lidar is the use of several mobile, short-range lidars. UAS surveys offer another promising approach to snowpack monitoring, providing high-resolution spatial data collection over large areas. However, there are several drawbacks to consider. UAS operations are often limited by weather conditions, flight time, and battery life, which can restrict the areas and timescales over which data can be collected. Additionally, regulatory restrictions and the need for skilled operators can pose significant challenges.

Recently, low-cost automotive lidar have been used statically for snow monitoring (Kapper and others, 2023; RSnowAUT-Konsortium, 2023; Ruttner-Jansen and others, 2024) and monitoring of a river bank (Perks and others, 2024). In this paper, we explore the feasibility of employing automotive lidars mounted on cable cars and ski lifts to increase spatial and temporal coverage. Currently, there are 24,256 ski lifts in operation across 6,148 ski resorts in the entire world (skiresort.at, 2023). Beyond recreational use, these lifts also play a essential role in urban transportation and in transporting vital goods, such as food and supplies, to remote mountain huts in the Alps. Consistently traveling the same routes over snow-covered landscapes, these lifts operate in areas frequently exposed to avalanche risks. The reduction in price and size of lidar sensors over the past decade has led to an increase in their popularity. Initially, their main market was the automotive industry, but many new applications have emerged. The wavelength of most automotive lidar systems is well-suited for snow and ice applications, as it is usually between 850nm and 903nm (Ous, 2021; Vel, 2018), where snow and ice are highly reflective (e.g. Hotaling and others, 2021).

In this study, we investigate the potential of permanent snow and ice monitoring from a lidar mounted on a cable car. Focus is put on 1.) the accuracy and precision of the snow surface detection, 2.) the influence of different mounting positions of the lidar on the gondola, 3.) the robustness of the SLAM algorithm to generate a cumulative point cloud from the moving lidar, 4.) investigate the potential errors introduced by vibrations and wind-induced movements of the cable car, and 5.) comparison between the lidar generated scan and the scans generated using UAS and TLSs. After a brief introduction to the study area, we first present our instrumentation and ground truth data, followed by the sections on data processing and results, and finally we end the paper with the discussions and conclusions.

(a) (b)

Fig. 1. Weather/snow conditions on the day of the survey: (a) View from the valley station towards the Hoher Sonnblick summit; (b) View from the gondola towards the valley station.

STUDY AREA

We performed the proof of concept measurements at Hoher Sonnblick in the Hohen Tauern mountain range in Salzburg, Austria. The Sonnblick Observatory, which is operated by the Austrian Meteorological Service, is located on its summit at around 3100m Above Seal Level (ASL). It stands out as a key site of several international atmospheric monitoring networks and has a continuous measurement series since 1886 (sonnblick.net, 2024). In 2018, the cable car from Kolm Saigurn (1624m ASL) to the observatory was rebuilt, making it possible to safely transport people and equipment, even at high winds. The cable car runs along the north-east side of the mountain over the length of 3054m, with a maximum speed of 6m/s. As the gondola is not open for public use, it provided us with the perfect opportunity for a field test. The measurement campaign took place on March 21, 2023, when the survey area was completely covered with snow, with a snow depth in the valley of about 85cm (see Figure 1).

INSTRUMENTATION

Main setup and measurement concept

The main setup is sketched in Figure 2. A sensor unit can be mounted on various moving components of a lift, such as

gondolas, chairs, or any other suitable part, to consistently and repeatedly measure the three-dimensional position of the snow surface. The sensor unit consists mainly of a lidar, an IMU, and a GNSS linked to a data-logger and power supply. However, the GNSS is optional, as satellite coverage is not always ideal in narrow mountain valleys (Kunisada and Premachandra, 2022). Therefore, ideally the SLAM algorithm together with GCPs should be enough to georeference the point cloud. The lidar can be a 360° rotating system, or have a more narrow field of view facing the snow surface below. Automotive lidars have frame rates of 10 to 20Hz, which is needed to avoid obstacles at speeds of 100km/h and more. This high frame rate together with the data from the GNSS and IMU is then used to generate a high-resolution cumulative point cloud using a SLAM algorithm.

Sensor system and mounting position

With only one support, the Sonnblick cable car ascends at a steep angle near the top with the summit couloir almost straight ahead. To also cover this part well, which is especially interesting in terms of snow avalanche activity, the lidar sensor, including the IMU, was mounted to the outside of the gondola facing the front and oriented obliquely downwards at an angle of approx. 37°. The GNSS antenna was mounted flat onto the roof of the gondola and all cables were routed to the cabin (see Figure S1 in the Supplements). For time synchronous recording of the sensor data, our custom logging unit MObile LIdar SENsor System (MOLISENS) running Ubuntu 20.04 and Robot Operating System (ROS) was used (for details on the system see (Goelles and others, 2022)). ROS enables time synchronous data logging from multiple sensors into one database file (rosbag) for simplified and standardized storage and data analysis. MOLISENS is a system integrating automotive lidars and optionally other automotive perception sensors independently from a complete vehicle setup, e.g., developed for autonomous or automated driving (Goelles and others, 2022). This makes it possible to use automotive lidar sensors also for other application domains, e.g., snowpack monitoring and glacier monitoring. Other than the sensors, MOLISENS consists of a data logger that is based on a Raspberry Pi 4 and external batteries. The used lidar, the Ouster OS2-64 Gen6, has a horizontal resolution of up to 2048 points in 360° and a vertical resolution of 64 points in 22.5°. The Ouster OS2-64 Gen6 rotates along the horizontal plane and achieves vertical resolution with 64 vertically aligned receivers, allowing frame rates of up to 20Hz.

Table 1. Instrument Overview

	Riegl VZ-6000	Ouster OS2	UAS
Max. Range	6000m	210m	N/A
Wavelength	1024nm	865nm	Visible light
Accuracy	±1.5cm at 150m	±3cm at 210m	±4cm
Method	Vertical line scan	SLAM	SFM

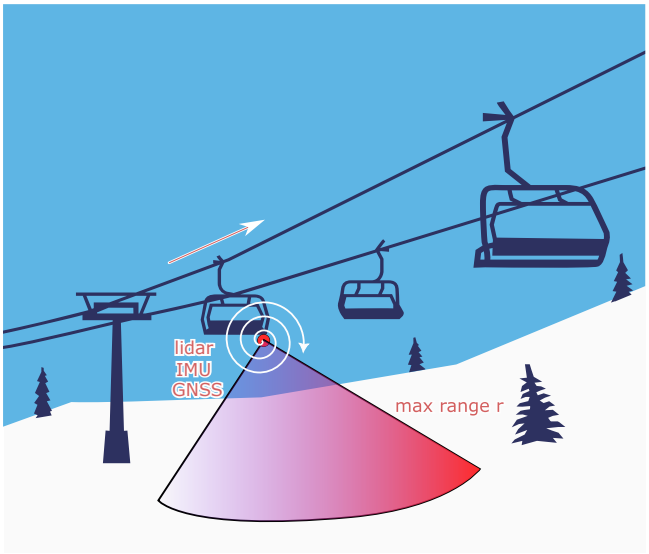

Fig. 2. Concept of the setup. A small rotating lidar (10 to 20Hz) is mounted on a gondola or chair. On the way up and/or down point cloud data is collected and then post-processed with a SLAM algorithm to get a cumulative point cloud. Then the snow free point cloud is subtracted to get the snow depth

Riegl VZ-6000 TLS

The Riegl VZ-6000 TLS is a high-end TLS that provides very detailed and accurate point clouds (including full-waveform information) with a range of up to 6000m, depending on visibility. The wavelength of the Riegl VZ-6000 is 1024nm and therefore well suited for snow and ice application, as well as for vegetation, soil, and gravel. The Riegl VZ-6000 applies a rotating scanner system with a single laser source and a single receiver device, hence each measurement point is recorded individually. A high precision gear box is used to move the scanner horizontally and a rotating mirror is redirecting the laser beam along the vertical axis. Compared to the MOLISENS sensor system, the Riegl VZ-6000 is significantly more expensive (order of € 100,000 - 200,000), larger

Fig. 3. Riegl VZ-6000 deployed at the bottom station of the cable car. Note the cables of the gondola which goes all the way up to the peak, where the Sonnblick Observatory is located. Also note the large number of occluded areas and the cliff.

and heavier (order of 10 - 20kg), less robust (IP64), and requires a very stable and solid tripod for operation in the field. A full high-resolution scan of an area comparable to the area investigated in this paper takes about an hour. This, together with the time and effort demanding set up, reduces typically the amount of view points significantly (e.g., in this paper, we consider only one view point for the Riegl) and thereby increases the occluded areas in the final scan (see Figure 3). The data quality in terms of accuracy and precision of the Riegl can be considered an order of magnitude better then the MOLISENS system.

UAS survey

On August 23, 2023, the survey area was mapped using a DJI Phantom 4 Pro UAS equipped with a Post-Processed Kinematic (PPK) Global Positioning System (GPS) extension. Due to the challenging topography of the study area, two different starting points were selected: one east of the Sonnblick Observatory and another at the base of the Sonnblick north face. To precisely reference the UAS images, ten GCPs were installed at the base of the wall and in the ridge area prior to the UAS flight. The flight encompassed six flight plans covering a total distance of approx. 30km. To avoid shadowing and ensure a comprehensive model of the entire investigated flank, images were captured both at nadir and perpendicular to the mean slope of the terrain. The target resolution for the imagery was set to 5cm. The surveyed area spanned approx. 1.2km^2, with elevations ranging from 2200 to 3100 meters ASL. During the mission, over 700 images were captured in raw data format. Uniform lighting conditions throughout the flight duration facilitated high data quality, with an average Root Mean Square (RMS) error of $\pm$4cm.

MOLISENS DATA PROCESSING

MOLISENS stores lidar data in a specific Ouster message format (ouster_ros/PacketMsg), not the standard ROS 3D point cloud format (sensor_msgs/PointCloud2). To use this data, a custom ROS package processes the raw data from a rosbag, saving the standardized output into a new rosbag. This new rosbag contains data in standard formats suitable for later processing. After preprocessing, the raw recorded data can be utilized in SLAM algorithms and for further analysis.

IMU and GNSS data analysis

Analyzing the IMU and GNSS data can unveil valuable information about the dataset itself, as well as the conditions under which the survey was performed. GNSS data, specifically, provides information about the latitude, longitude, and the altitude of the sensor throughout the survey. Visualizing this data not only provides a clear picture of the sensor's trajectory but also facilitates the detection of any anomalies within the dataset that warrant closer scrutiny. IMU data is even more valuable, since it provides information about external forces, i.e. wind, cable bending, etc., affecting the motion and stability of the sensor system. These can be visualized and inspected on the linear acceleration and angular velocity plots. The plots can show the values over time, or, by using Fast Fourier Transformation (FFT), the data can be converted into the single spectral components, thus providing frequency information about the individual IMU data. This frequency information provides more information about the nature of external forces that are affecting the sensor system. For the analysis of the IMU and GNSS

data, two custom packages are used. First, a ROS package extracts the data from the rosbag containing all the raw data. Subsequently, a MATLAB package is used to process and visualize the data.

SLAM algorithms

There exists a multitude of different lidar SLAM methods and techniques, as mentioned in Dikic (2023). For our application, we considered only the algorithms that are open-source, available for ROS, and do not specifically require GNSS data to work. These criteria have narrowed down our choice to four possible algorithms, KISS-ICP (Vizzo and others, 2022), LeGO-LOAM (Shan and Englot, 2018), HDL-Graph-SLAM (Koide and others, 2019), and LIO-SAM (Shan and others, 2020). The main goal is to strike a balance between the quality of the 3D point cloud and the speed and simplicity of its construction. To achieve this, algorithms based on different technologies are implemented. These algorithms can be divided into two types of SLAM algorithms: odometry and mapping algorithms and full SLAM algorithms. The key distinction is that odometry estimates position incrementally, frame by frame, while full SLAM approaches aim to maintain global consistency by detecting revisited places and correcting pose estimation errors through loop-closure detection (Dikic, 2023). As research by (Dikic, 2023) shows, all SLAM algorithms except LIO-SAM have deficiencies in snow-covered environments. Therefore, only LIO-SAM is considered. LIO-SAM uses a 3D lidar, IMU, and optionally GNSS for sensor state and trajectory estimation. It employs a factor graph with IMU pre-integration, lidar odometry, GNSS, and loop-closure factors, optimizing the graph with incremental smoothing. This system effectively manages IMU bias and noise, reduces drift with GNSS, and corrects altitude errors, providing precise sensor state estimation and mapping (Shan and others, 2020).

SLAM 3D point cloud is received as an output of the LIO-SAM algorithm. Due to the complexity and range of the surveyed terrain, the rosbag playback factor was reduced to 0.25, which means that each second of recorded data took 4 seconds to be fed to the LIO-SAM algorithm. Furthermore, given the distances between distinct features at some places in the environment, the SLAM algorithm may fail, so it is desirable to split the mapping process, thus the overall 3D point cloud, into smaller sections. These sections are later stitched into a complete 3D point cloud of the environment.

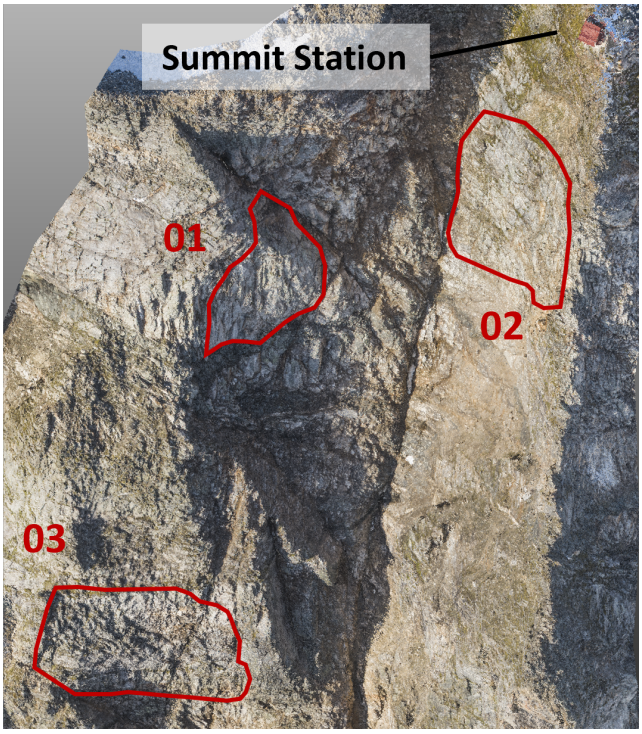

Fig. 4. UAS data (Structure from motion (SfM)) of the steep rock face (23.08.2023) located in the summit couloir of Hoher Sonnblick used for comparison with MOLISENS data. The three red circled areas have been generally snow free and act as the references.

Vegetation removal algorithm

The 3D point cloud produced by the SLAM algorithm represents a Digital Surface Model (DSM), capturing all environmental features scanned by the lidar sensor. However, vegetation can increase errors in lidar scans due to laser pulse scattering (Su and Bork, 2006) and cause alignment issues between 3D point clouds of the same area due to movement (Dikic, 2023). Measuring snow depth is easier with a Digital Terrain Model (DTM) instead of a DSM. To address this, a Cloth Simulation Filter (CSF) (Zhang and others, 2020) is used to remove vegetation from the SLAM-generated 3D point clouds. The CSF method, based on "Cloth simulation-based construction of pit-free Canopy Height Models (CHMs)" developed by Zhang and others, simulates interactions between a virtual cloth and lidar data points to estimate canopy heights. This process results in two point clouds: one containing only the vegetation and another one representing the DTM.

Scan quality and sources of uncertainty

To evaluate the overall quality of the generated DSMs and DTMs, we need to assess aspects of point cloud precision and accuracy. Due to a lack of GCPs in the difficult-to-access study area, we must acquire these measures by comparing pairs of point clouds. Precision, or repeatability, can be investigated by comparing the MOLISENS measurements from two distinct cable car rides taken on the same day with the same setup. Therefore we compare measurements 2 and 4 from the Table 2, as in both cases the mounting of the sensor and the amount of passengers on board were the same. To estimate accuracy, i.e., deviation from a known reference, a reference scan is required. This process is more complex, and multiple sources of uncertainty must be considered to estimate the overall system uncertainty. These sources include sensor accuracy, uncertainties in the SLAM calculation, point cloud registration uncertainty, and confidence in the reference scan itself.

In our case, the reference scan can be assumed to be an order of magnitude more accurate, thus acting as ground truth. As described in Table 1, sensor accuracy falls within the millimeter to centimeter range, which is significantly lower than the overall uncertainty, which will be discussed later. This means the two largest sources of uncertainty are the LIO-SAM SLAM algorithm and the registration process. The alignment method for fine registration, is the commonly known Iterative Closest Point (ICP) (Chen and Medioni, 1992), which is implemented in the open-source point cloud manipulation software CloudCompare. ICP outputs a single RMS value that provides at least some information on the quality of the alignment, while LIO-SAM does not come with any inherent confidence measure.

Aligning two scans utilizing ICP proves to be highly effective when minimal change is present between them. However, the alignment process becomes significantly more challenging when comparing a scan devoid of snow to one that includes snow coverage. One approach is to exclude snow-covered areas from the UAS scan and align the remaining snow free areas with the reference. Then, the resulting transformation matrix can be used to align the full scan. However, the smaller the snow-free areas, the more challenging it becomes to achieve a good fit. Vegetation presents another challenge. Even though it can be removed from the snow-free reference scan by calculating a DTM, this is not possible in the snow covered case and the vegetation becomes increasingly compressed under heavier snow loads. To mitigate this limitation, a steep area with minimal vegetation and predominantly rocks near the summit was selected for the accuracy assessment. First, the larger snow patches were removed from the MOLISENS scan; then the MOLISENS and UAS data were registered; and finally, three individual rock faces were extracted and used for comparison (see Figure 4). The transformation matrix of the cropped scan can than be applied to the full scan to visualize snow accumulation zones.

Comparison of 3D point clouds

To compare two point clouds and calculate the error of the test scan, the Multiscale Model to Model Cloud Comparison (M3C2) algorithm (Lague and others, 2013) for calculating cloud-to-cloud distances, which is built into CloudCompare, is used. The M3C2 algorithm is a powerful tool for computing robust and signed distances between two point clouds. It focuses on specific points known as core points, which are sub-sampled versions of the original reference point cloud and represent regions of interest. M3C2 operates in two essential steps: first, it calculates normal vectors for each core point, and then it projects these points onto each cloud using cylindrical projections along the normal direction. This projection process results in distance distributions that provide valuable insights into point cloud roughness and average positions. The final distance between the two point clouds is determined based on these distributions. M3C2 is specifically designed for dense point clouds and proves especially useful for analyzing complex topographies (e.g. Lague and others, 2013; Iglseder, 2018).

For estimating the point cloud accuracy using the M3C2 method, several steps are involved. Initially, manual alignment of the reference point cloud and the SLAM 3D point cloud is performed, followed by precise alignment using the ICP algorithm with customizable constraints. Subsequently, M3C2 calculates distances along the normal direction between the two point clouds. Additionally, the algorithm estimates a 95% confidence interval at the projection scale. This interval accounts for the point cloud roughness and registration error and is returned as distance uncertainty, providing a measure of the reliability of the distance calculation. It can be used to assess whether a statistically significant change has occurred at a specific location on the surface.

RESULTS

For this study, four measurement runs with the MOLISENS system and one VZ-6000 scan were conducted. The reference data without snow cower was recorded at a

Table 2. Details about conducted measurements

	Meas.1	Meas.2	Meas.3	Meas.4
mounting	horizontal	vertical	vertical	vertical
direction	up & down	up	down & up	down
passengers	with	with	without	with
approx. time	11:45AM	12:45PM	01:30PM	02:00PM
wind sp. in m/s	4.55	3.65	3.30	3.30
violin color	blue	orange	yellow	purple

later date by an UAS. The specifics of the four MOLISENS conducted measurements are listed and described in Table 2.

IMU and GNSS data analysis

The GNSS data analysis, while necessary, merely confirms the accuracy of altitude, latitude, and longitude readings from the GNSS module (see Figure S3). In contrast, the data from the IMU offers much more intriguing insights.

Figure 5 shows the violin plots of the linear acceleration in x-, y-, and z-direction of the OS2-64 of the four measurements. It can be seen that the yellow plot of measurement 3 differs from the other measurements in terms of the representation of the linear acceleration in the x-direction. This difference is probably caused since measurements 1, 2, and 4 were conducted with passengers in the cable car whereas measurement 3 took place without them, i.e., the gondola sways more in x-direction when it is empty. Furthermore, in y-direction, the spread of measured linear accelerations is larger for measurement 1 compared to the other measurements. This effect is probably caused by a higher wind speed during measurement 1 compared to

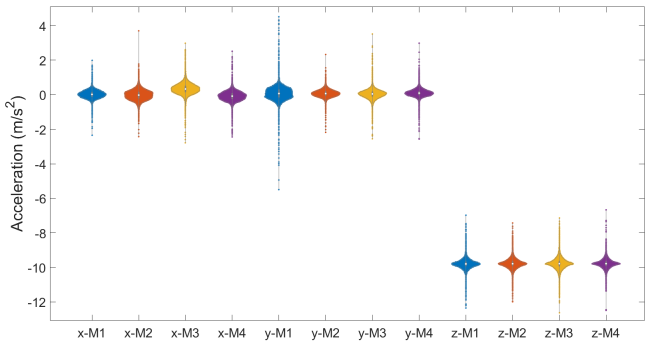

Fig. 5. Comparison of linear acceleration violin plots in x-, y-, and z-direction over four different measurement runs. Specifics of each run are given in Table 2. M stands for measurement

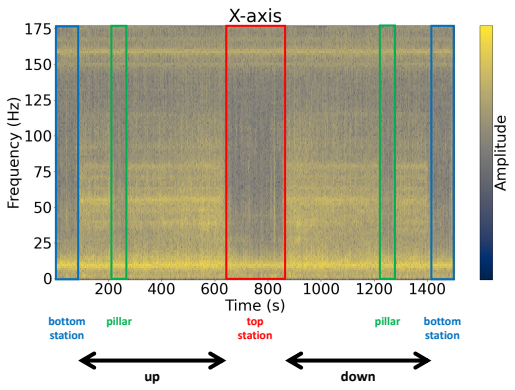

Fig. 6. Spectrogram of the linear acceleration for the x-axis with the lidar mounted horizontally

measurements 2, 3, and 4 since the gondola sways more in y-direction, i.e., to the left and the right, when a higher wind speed acts on the gondola.

The FFTs of the linear acceleration in x-, y-, and z-direction are shown in Figure S4. Each FFT shows a peak at 10Hz. These peaks are probably caused by the rotation frequency of the mirror of the OS2 -64 which was chosen with 10Hz. The spectrogram for each axis is shown in Figure S2 where the x-axis shows the time and the y-axis the FFT per timestamp.

A more detailed view of just the x-axis is shown in Figure 6. During this measurement, the gondola ascended once and then descended again. The gray area between approx. 600s and 800s is the time where the gondola was stationary at the top station. There is one pillar for the cable between the bottom station and the top station. In Figure 6, at about 250s and 1250s there is also a gray area similar to the one where the gondola was stationary. The gondola reached the pillar at these two points in time, once on the way up and once on the way down. These frequencies, which are present only when the cable car is moving, are probably caused by the vibrations of the cable and movements of the gondola because of wind. It can be observed that the frequency at 10Hz is present at the entire time of measurement. This confirms the assumption that the frequency of 10Hz is caused by the rotation frequency of the mirror in the lidar, as it continues to rotate even when stationary and when passing the pillar.

SLAM 3D point cloud

As mentioned previously, we used LIO-SAM to generate a comprehensive 3D point cloud of the entire survey area. Necessitated by the survey's complexity, nine separate point clouds were generated for the entire survey area. This division was more frequent in the central part of the survey area due to the lower number of scanned distinct features there. During post-processing, these nine sections were meticulously stitched together to form a single 3D point cloud. However, this stitching process is both tedious and complex, often resulting in unavoidable and undesired artifacts. These artifacts, visible as dark arcs in Figure 7, indicate areas with a lower density of points in the 3D point cloud.

Figure 7 shows the area surrounding the cable car to the Hoher Sonnblick observatory. This 3D point cloud is georeferenced to an orthophoto, and two details show the areas of interest for quality assessment. The total number of points in the final 3D point cloud is over 43 million, proving that the combination of MOLISENS and LIO-SAM yields higher resolution maps compared to other combinations explored in Dikic (2023). In the following section, the mentioned top and bottom parts of this 3D point cloud are analyzed in more detail and compared with our reference 3D point cloud to determine whether the accuracy and precision of the SLAM 3D point cloud are sufficient for the intended applications outlined in the introduction.

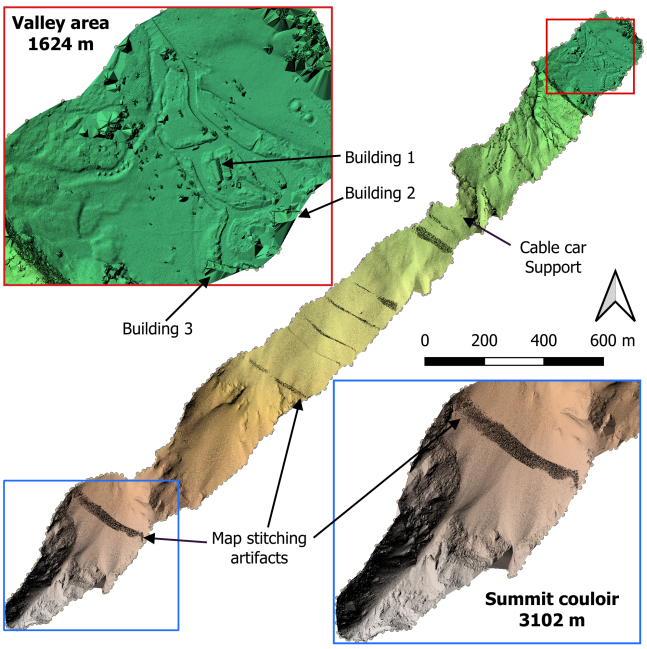

Fig. 7. DTM of the entire survey area with two detailed views of the valley area of Kolm Saigurn (red) and the couloir directly below the Sonnblick summit (blue). The dark arcs are artifacts created by merging the individual 3D SLAM generated point clouds. They can be seen particularly clearly halfway up the profile, where there are no distinct features that are essential for the calculation.

Quality assessment

This section presents the results of the quality assessment. For the accuracy assessment, only the data from the UAS is used as ground truth. Despite the high quality of the Riegl VZ-6000 3D point cloud, it contains a large number of occluded areas (see Figure S5), which means it does not fully represent the entire survey area. This is particularly problematic in the area of interest near the summit, where the occlusions significantly limit the data's usefulness. Therefore, to ensure a comprehensive and accurate assessment, the UAS data was exclusively utilized.

Precision

The lower segment of the full scan, extending from the valley station to the cable car support pillar, was selected to evaluate the repeatability of our methodology. SLAM succeeded in generating a continuous 3D point cloud for this area, which encompasses both complex terrain featuring buildings and vegetation, and uniform sections covered in snow. For the majority of the 3D point cloud, distance values re-

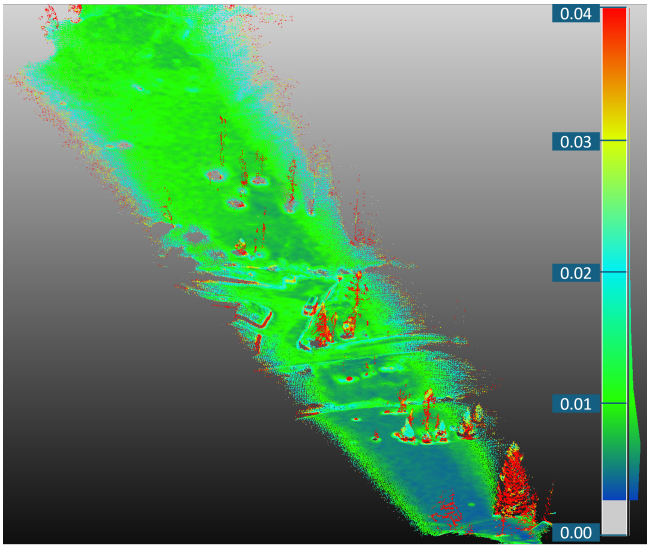

Fig. 8. Point cloud of M3C2 distance uncertainty in meter between two separate cable car rides using MOLISENS.

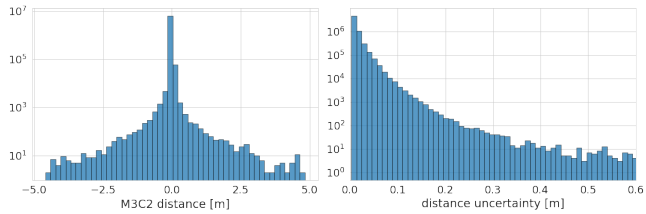

Fig. 9. M3C2 distance (left) and distance uncertainty (right) distribution when comparing two point clouds created with MOLISENS. Note that the y-scale is logarithmic.

side within the centimeter range, aligning with the sensor's range accuracy. Larger values are predominantly observed in areas of vegetation and surfaces aligned with the lidar's view, yet these remain far below 10 cm in most instances. The distribution of M3C2 distances (Mean: −0.0002m, STD: 0.0328m) along with the associated distance uncertainties (Mean: 0.0129m, STD: 0.0134m) are presented in Figure 9. Figure 8 illustrates a portion of the resulting 3D point cloud, colored according to M3C2 distance uncertainty. Notably, distance uncertainties (as well as distances) begin to increase towards the scan's periphery, a phenomenon largely attributable to the decreasing density of the 3D point cloud in these regions. No significant correlation is observed between distance uncertainty and M3C2 distance, or the distance-from-center-line (defined as the distance from a point to a vertical plane along the cable car rope). However, a slight and anticipated increase in uncertainty is noted with greater distance-from-center-line, as well as with increased M3C2 distance. Overall, the findings indicate exceptional repeatability of our system, suggesting that a permanent monitoring solution could effectively detect even minor variations in snow depth.

Accuracy

While precision is more important for detecting day to day changes we also investigated the accuracy of our scans when compared to a known ground truth. Figure 10 shows the distributions of M3C2 distances and M3C2 distance uncertainties for the three selected rock walls from Figure 4. While the distributions vary slightly between rock walls it is clear that uncertainties are much higher in this case. The standard deviation for M3C2 distance ranges from 0.33m of rock wall 02 to 0.57m for rock wall 03. While mean values for rock wall 02 and 03 are close to zero (0.06m and 0.004m) rock wall 01 has a mean of −0.23m which indicates an alignment problem in this area. The standard deviations for M3C2 distance uncertainties range from 0.01m to 0.03m. Distance uncertainty values starting at 0.93m is due to the propagated registration error which is accounted for by the M3C2 algorithm (see Eq. 1 in Lague and others (2013)). Considering the higher mean value for rock wall 01, the error varies in the different parts of the compared areas and likely increases with larger scans. The considerable standard deviation, on the other hand, suggests that differences are not uniformly distributed across the compared areas. Upon closer examination of the resulting difference point clouds, it appears that this variability predominantly originates from small snow patches still present in the selected test areas. As described, it is challenging to attribute the resulting uncertainty values specifically to either the registration process or the SLAM algorithm. By investigating these factors more thoroughly in the future, we aim to enhance the overall accuracy. Despite these issues, the mean and standard deviation values of the error are sufficiently low to support further analysis of the survey area.

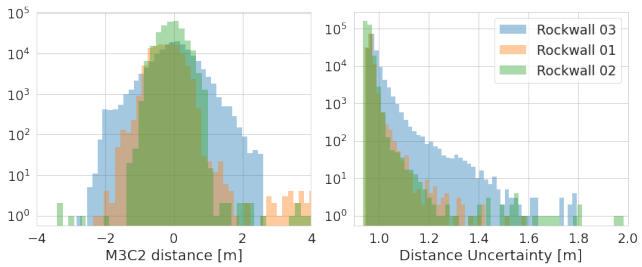

Fig. 10. M3C2 distance (left) and distance uncertainty (right) distribution for three snow free rock faces when comparing MOLISENS with the reference data. Note that the y-scale is logarithmic.

Snow depth map

The resulting snow depth estimate for the top area of the Sonnblick is depicted in Figure 11. This map was created using two different data sources (MOLISENS and UAS as a reference), which introduces some inaccuracies as discussed in the preceding chapters. Nevertheless, it presents a generally realistic depiction and provides a good impression of what could be achieved with a permanent scanning setup monitoring daily snow depth changes. As shown, the largest snow accumulations are found in the large snow patch at the base of the cliff and in the couloir, reaching up to 5 meters.

DISCUSSION AND CONCLUSIONS

The initial trials of our novel approach showed very promising results. Although some difficulties were faced, overall the method is viable as it is possible to create a high

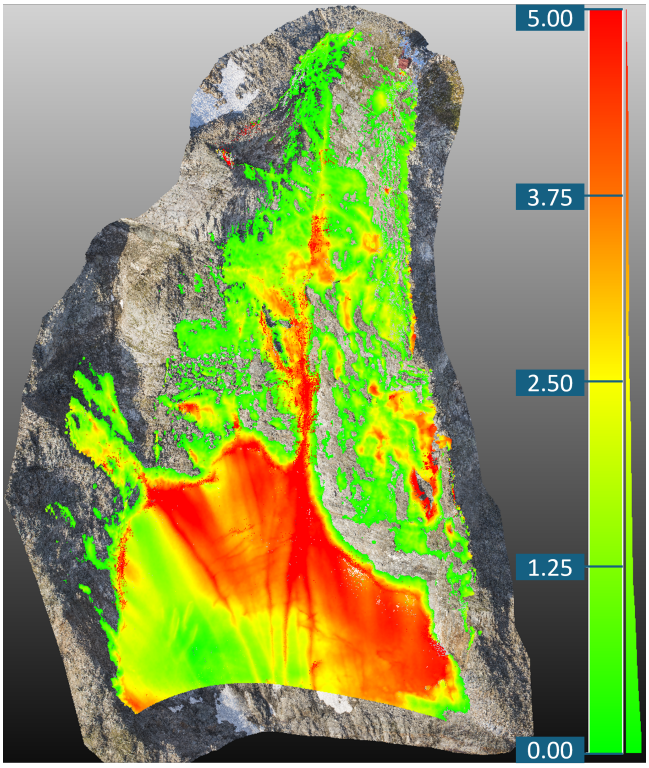

Fig. 11. Snow depth in the summit couloir of Hoher Sonnblick in meters calculated by comparison of MOLISENS scan from 21 March 2023 and UAS data from 23 of August 2023. The true color 3D point cloud in the background is the reference UAS data and the green to red colored 3D point cloud represents the calculated snow depth. Depths of up to 5 meters can be found at the base of the cliffs and inside couloir.

resolution 3D SLAM point cloud of the study area, with an accuracy comparable to the reference 3D point clouds. Figure S6 shows parts of the SLAM-generated 3D point cloud on an image of the same area taken from Google maps.

One of the main issues we faced was the inability to create a full 3D point cloud in one run of the SLAM algorithm. This forced us to create smaller 3D point cloud segments and then later stitch them together. Another issue, is the ever-present 10Hz noise, which arises from the rotation of the lidar sensor itself. We believe that this noise affects the SLAM process and that it can be reduced, or even completely eliminated, with improved mounting techniques or new solid state lidar technologies. Ultimately, the fact that LIO-SAM is unable to create a continuous 3D point cloud of the full scene, due to the factors such as noise and monotony of the scene itself is an issue that needs to be addressed. One of the solutions, besides improving the mounting system, would be to use a longer range lidar, in order to capture more distinct features at higher distances to make the SLAM process easier. E.g., the new Livox Avia sensor has a range of 450m and is well suited for snow and ice measurements given its operating wavelength at 905nm (Livox Technology, 2024). Further increasing the lidar range up to one or several km would currently require a substantial financial investment, since high range lidars systems are still relatively expensive (order of € 100,000). Another approach is to adapt the SLAM algorithm with extra constraints specific to our use case, or to use a better SLAM algorithm, such as commercially available solutions. For further investigation, it might be good to compare it with a solution from, e.g., Exwayz or Kudan (exwayz.fr, 2024; kudan.io, 2024). These two companies provide SLAM algorithms designed for large-scale mapping, so they also use different sensor data, like lidar, IMU and GNSS, and fuse these signals. These solutions also provide a georeferenced 3D point cloud using GNSS. Furthermore, a robust solution for comparing two scans must be developed. The installation of GCPs could greatly assist in this process. Specifically, the registration process needs to become more accurate, as well as simpler and more streamlined, to reliably measure snow depth differences.

Our next steps will include the integration of a camera into our system to further improve the creation of the 3D map and classification based on lidar - camera sensor fusion (e.g., autoware, SLAM+SFM, fixed position between lidar and camera, etc.). The SLAM performance can be further improved by adding lidar and/or camera targets into the field that the algorithm can find and locate. This can potentially remove the artifact lines that are visible as dark lines in the current point cloud.

Consumer grade lidar are currently not suitable for applications on the gondola as their range is still relatively low, e.g., the iPhone 15 Pro lidar has a range of about 5m. Nevertheless, the high accuracy and low price of consumer grade lidar make them well suitable for snow observations in general as shown, e.g., in (King and others, 2023). Additionally, UAS based solid-state LiDAR sensors, e.g., the DJI Zenmuse L1 UAS uses the Livox Avia sensor with range of up to 450m (DJI, 2023; Livox Technology, 2024), show very promising results for creating elevation models even in vegetation-rich terrains (MacDonell and others, 2023), underscoring the need for context-aware deployment.

SUPPLEMENTARY MATERIAL

The supplementary material for this article can be found at ...

ACKNOWLEDGMENTS

The project RSnowAUT was funded by the program "Austrian Space Applications Programme (ASAP)" of the Austrian Federal Ministry for Climate Action (BMK). The Austrian Research Promotion Agency (FFG) has been authorised for the programme management. The publication was partly written at Virtual Vehicle Research GmbH in Graz and partially funded within the COMET K2 Competence Centers for Excellent Technologies from the Austrian Federal Ministry for Climate Action (BMK), the Austrian Federal Ministry for Labour and Economy (BMAW), the Province of Styria (Dept. 12) and the Styrian Business Promotion Agency (SFG). The authors acknowledge the financial support by the University of Graz and the Virtual Vehicle Research GmbH. We acknowledge the Sonnblick Observatory of GeoSphere Austria for providing Access to the Research Infrastructure. The work of Pedro Batista was supported by LARSyS FCT funding (DOI: 10.54499/LA/P/0083/2020, 10.54499/UIDP/50009/2020, and 10.54499/UIDB/50009/2020)

REFERENCES

(2018) *Velodyne LiDAR PUCK - REAL-TIME 3D LiDAR SENSOR*. Velodyne LiDAR, Inc.

(2021) *OS1 Mid-Range High-Resolution Imaging Lidar*. Ouster, Inc., rev: 2/11/2021

Beniston M, Farinotti D, Stoffel M, Andreassen LM, Coppola E, Eckert N, Fantini A, Giacona F, Hauck C, Huss M, Huwald H, Lehning M, López-Moreno JI, Magnusson J, Marty C, Morán-Tejéda E, Morin S, Naaim M, Provenzale A, Rabatel A, Six D, Stötter J, Strasser U, Terzago S and Vincent C (2018) The european mountain cryosphere: a review of its current state, trends, and future challenges. *The Cryosphere*, **12**(2), 759–794 (doi: 10.5194/tc-12-759-2018)

Bühler Y, Marty M, Egli L, Veitinger J, Jonas T, Thee P and Ginzler C (2015) Snow depth mapping in high-alpine catchments using digital photogrammetry. *The Cryosphere*, **9**(1), 229–243 (doi: 10.5194/tc-9-229-2015)

Chen Y and Medioni G (1992) Object modelling by registration of multiple range images. *Image and Vision Computing*, **10**(3), 145–155, ISSN 0262-8856 (doi: 10.1016/0262-8856(92)90066-C)

Deems JS, Painter TH and Finnegan DC (2013) Lidar measurement of snow depth: a review. **59**(215), 467–479 (doi: 10.3189/2013jog12j154)

Dikic B (2023) *Automotive Lidar Technology for Marine Applications – Determining and Increasing the Accuracy of Simultaneous Localisation and Mapping*. Master's thesis, Instituto Superior Técnico, Universidade de Lisboa, Portugal (doi: 10.13140/RG.2.2.10942.46406)

DJI (2023) Zenmuse l1 - specs. `https://enterprise.dji.com/de/zenmuse-l1/specs`, accessed: 2024-01-19

exwayzfr (2024) exwayz unleash 3d lidar power

Goelles T, Hammer T, Muckenhuber S, Schlager B, Abermann J, Bauer C, Expósito Jiménez VJ, Schöner W, Schratter M, Schrei B and Senger K (2022) Molisens: Mobile lidar sensor system to exploit the potential of small industrial lidar devices for geoscientific applications. *Geoscientific Instrumentation, Methods and Data Systems*, **11**(2), 247–261 (doi: 10.5194/gi-11-247-2022)

Hotaling S, Lutz S, Dial RJ and others (2021) Biological albedo reduction on ice sheets, glaciers, and snowfields. **220**, 103728, ISSN 0012-8252 (doi: 10.1016/j.earscirev.2021.103728)

Iglseder A (2018) *Detection of surface changes using terrestrial laser scanning: A field study on rock instabilities in the Ybbs Valley, Lower Austria*. Master's thesis, University of Vienna, Austria

Kapper K, Goelles T, Muckenhuber S, Trügler A, Abermann J, Schlager B, Gaisberger C, Eckerstorfer M, Grahn J, Malnes E, Prokop A and Schöner W (2023) Automated snow avalanche monitoring for austria: State of the art and roadmap for future work. *Frontiers in Remote Sensing*, **4**, 1156519 (doi: 10.3389/frsen.2023.1156519)

King F, Kelly R and Fletcher CG (2023) New opportunities for low-cost lidar-derived snow depth estimates from a consumer drone-mounted smartphone. *Cold Regions Science and Technology*, **207**, 103757, ISSN 0165-232X (doi: 10.1016/j.coldregions.2022.103757)

Koide K, Miura J and Menegatti E (2019) A portable three-dimensional lidar-based system for long-term and wide-area people behavior measurement. *International Journal of Advanced Robotic Systems*, **16** (doi: 10.1177/1729881419841532)

kudanio (2024) Frontier on commercial-grade localization mapping software

Kunisada Y and Premachandra C (2022) High precision location estimation in mountainous areas using gps. *Sensors*, **22**(3), ISSN 1424-8220 (doi: 10.3390/s22031149)

Lague D, Brodu N and Leroux J (2013) Accurate 3d comparison of complex topography with terrestrial laser scanner: Application to the rangitikei canyon (n-z). *ISPRS Journal of Photogrammetry and Remote Sensing*, **82**, 10–26, ISSN 0924-2716 (doi: https://doi.org/10.1016/j.isprsjprs.2013.04.009)

Livox Technology (2024) Livox avia specifications. `https://www.livoxtech.com/avia/specs`, accessed: 2024-01-19

MacDonell CJ, Williams RD, Maniatis G, Roberts K and Naylor M (2023) Consumer-grade uav solid-state lidar accurately quantifies topography in a vegetated fluvial environment. *Earth Surface Processes and Landforms*, **48**(11), 2211–2229, ISSN 1096-9837 (doi: 10.1002/esp.5608)

Marty C (2013) *Climate change and snow cover in the European Alps*, 33–44. ISBN 978-1-60805-632-3

Perks M, Pitman S, Bainbridge R, Diaz Moreno A and Dunning S (2024) An evaluation of low-cost terrestrial lidar sensors for assessing geomorphic change. In *EGU General Assembly 2024*, Vienna, Austria, eGU24-19935

Pesci A, Teza G and Bonali E (2011) Terrestrial laser scanner resolution: Numerical simulations and experiments on spatial sampling optimization. *Remote Sensing*, **3**(1), 167–184, ISSN 2072-4292 (doi: 10.3390/rs3010167)

Rixen C, Høye TT, Macek P, Aerts R, Alatalo JM, Anderson JT, Arnold PA, Barrio IC, Bjerke JW, Björkman MP, Blok D, Blume-Werry G, Boike J, Bokhorst S, Carbognani M, Christiansen CT, Convey P, Cooper EJ, Cornelissen JHC, Coulson SJ, Dorrepaal E, Elberling B, Elmendorf SC, Elphinstone C, Forte TG, Frei ER, Geange SR, Gehrmann F, Gibson C, Grogan P, Halbritter AH, Harte J, Henry GH, Inouye DW, Irwin RE, Jespersen G, Jónsdóttir IS, Jung JY, Klinges DH, Kudo G, Lämsä J, Lee H, Lembrechts JJ, Lett S, Lynn JS, Mann HM, Mastepanov M, Morse J, Myers-Smith IH, Olofsson J, Paavola R, Petraglia A, Phoenix GK, Semenchuk P, Siewert MB, Slatyer R, Spasojevic MJ, Suding K, Sullivan P, Thompson KL, Väisänen M, Vandvik V, Venn S, Walz J, Way R, Welker JM, Wipf S and Zong S (2022) Winters are changing: snow effects on arctic and alpine tundra ecosystems. *Arctic Science*, **8**(3), 572–608, ISSN 2368-7460 (doi: 10.1139/as-2020-0058)

Robert S, Daniel S, Bruno A, Marc P and Carlo A (2019) A critical review of climate change risk for ski tourism. *Current Issues in Tourism*, **22**(11), 1343–1379 (doi: 10.1080/13683500.2017.1410110)

RSnowAUT-Konsortium (2023) Das potential von automobilsensoren für die lokale detektion von lawinen im rahmen des ffg-projekts rsnowaut. In *5. Lawinensymposium Graz 2023*, ISBN 978-3-903252-18-9

Ruttner-Jansen P, Voordendag A, Hartmann T, Glaus J, Wieser A and Bühler Y (2024) Monitoring snow depth variations in an avalanche release area using low cost lidar and optical sensors. *EGUsphere*, **2024**, 1–20 (doi: 10.5194/egusphere-2024-744)

Shan T and Englot B (2018) Lego-loam: Lightweight and ground-optimized lidar odometry and mapping on variable terrain. In *2018 IEEE/RSJ International Conference on Intelligent Robots and Systems (IROS)*, 4758–4765 (doi: 10.1109/IROS.2018.8594299)

Shan T, Englot B, Meyers D, Wang W, Ratti C and Rus D (2020) Lio-sam: Tightly-coupled lidar inertial odometry via smoothing and mapping

skiresortat (2023) Skilifte weltweit

sonnblicknet (2024) Data

Su J and Bork E (2006) Influence of vegetation, slope, and lidar sampling angle on dem accuracy. *Photogrammetric Engineering & Remote Sensing*, **72**(11), 1265–1274, ISSN 0099-1112 (doi: doi: 10.14358/PERS.72.11.1265)

Vizzo I, Guadagnino T, Mersch B, Wiesmann L, Behley J and Stachniss C (2022) Kiss-icp: In defense of point-to-point icp - simple, accurate, and robust registration if done the right way. *ArXiv*, **abs/2209.15397**

Voordendag A, Prinz R, Schuster L and Kaser G (2023) Brief communication: The glacier loss day as an indicator of a record-breaking negative glacier mass balance in 2022. *The Cryosphere*, **17**(8), 3661–3665, ISSN 1994-0424 (doi: 10.5194/tc-17-3661-2023)

Voordendag AB, Goger B, Klug C and others (2022) The stability of a permanent terrestrial laser scanning system - a case study with hourly scans. volume 43, 1093–1099, International Society for Photogrammetry and Remote Sensing, ISSN 16821750 (doi: 10.5194/isprs-archives-XLIII-B2-2022-1093-2022)

Zhang W, Cai S, Liang X, Shao J, Hu R, Yu S and Yan G (2020) Cloth simulation-based construction of pit-free canopy height models from airborne lidar data. *Forest Ecosystems*, **7**, 1 (doi: 10.1186/s40663-019-0212-0)

Supplementary material of: "Lidar-based snow monitoring: cable car deployment in the Austrian Alps"

B. Dikic, T. Goelles, C. Gaisberger, B. Schlager, S. Muckenhuber, P. Batista, M. Keuschnig, and M. Schratter

Correspondence to: T. Goelles (thomas.goelles@uni-graz.at) and B. Dikic (berin.dikic@v2c2.at)

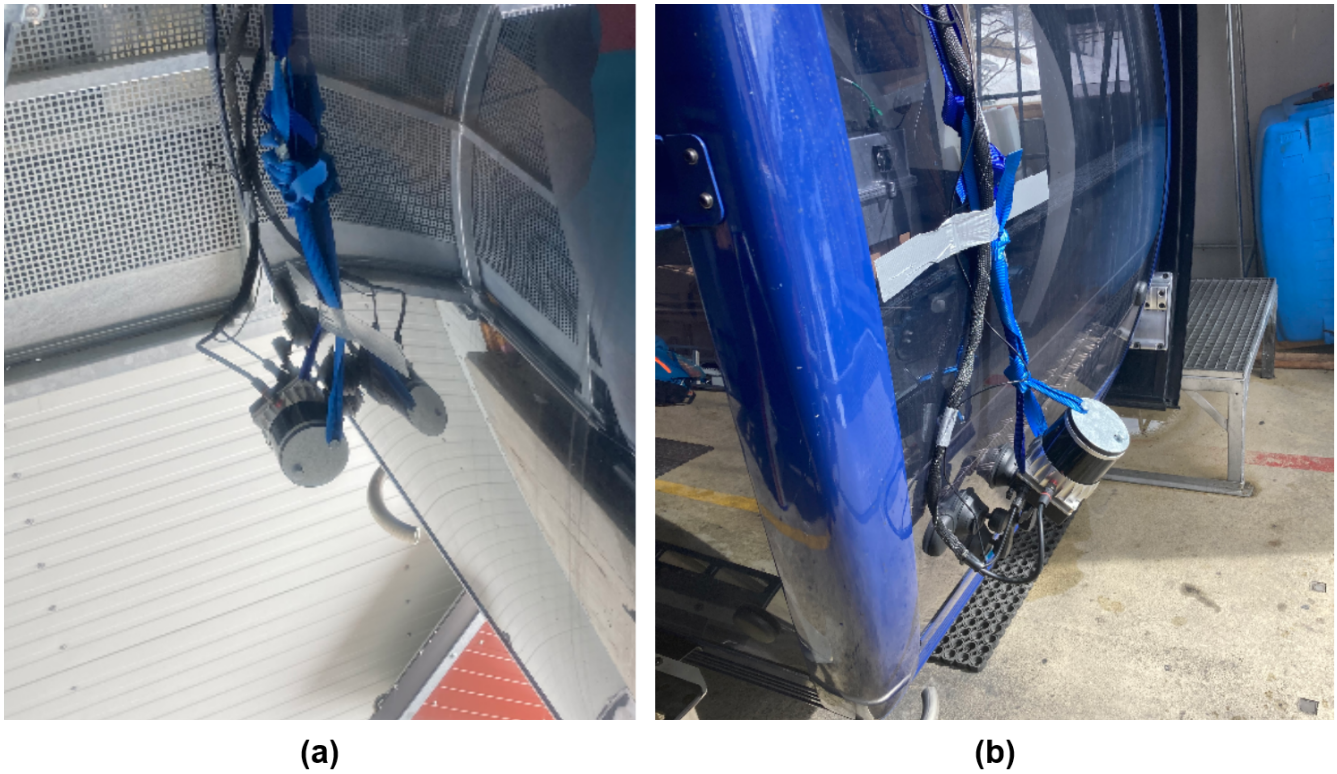

Fig. S1. MOLISENS lidar sensor mounting styles: (a) Vertically scanning lidar, used for the first three measurements; (b) Horizontally scanning lidar, used for the final measurement

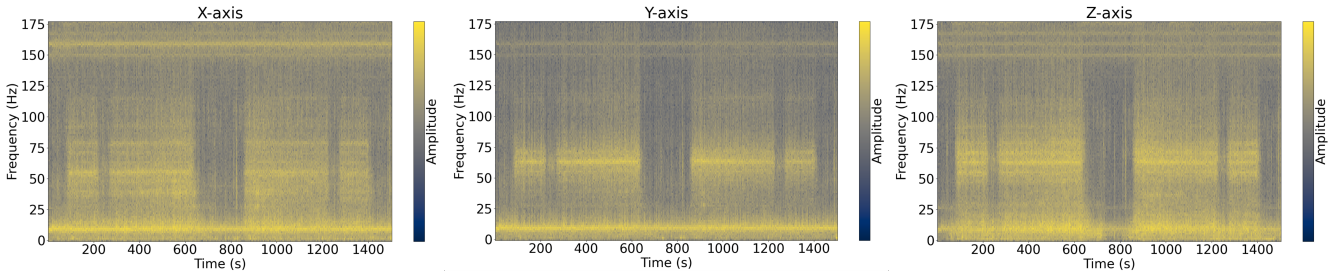

Fig. S2. Spectrogram of the linear acceleration for the x-, y-, and z-axis with the lidar mounted horizontally

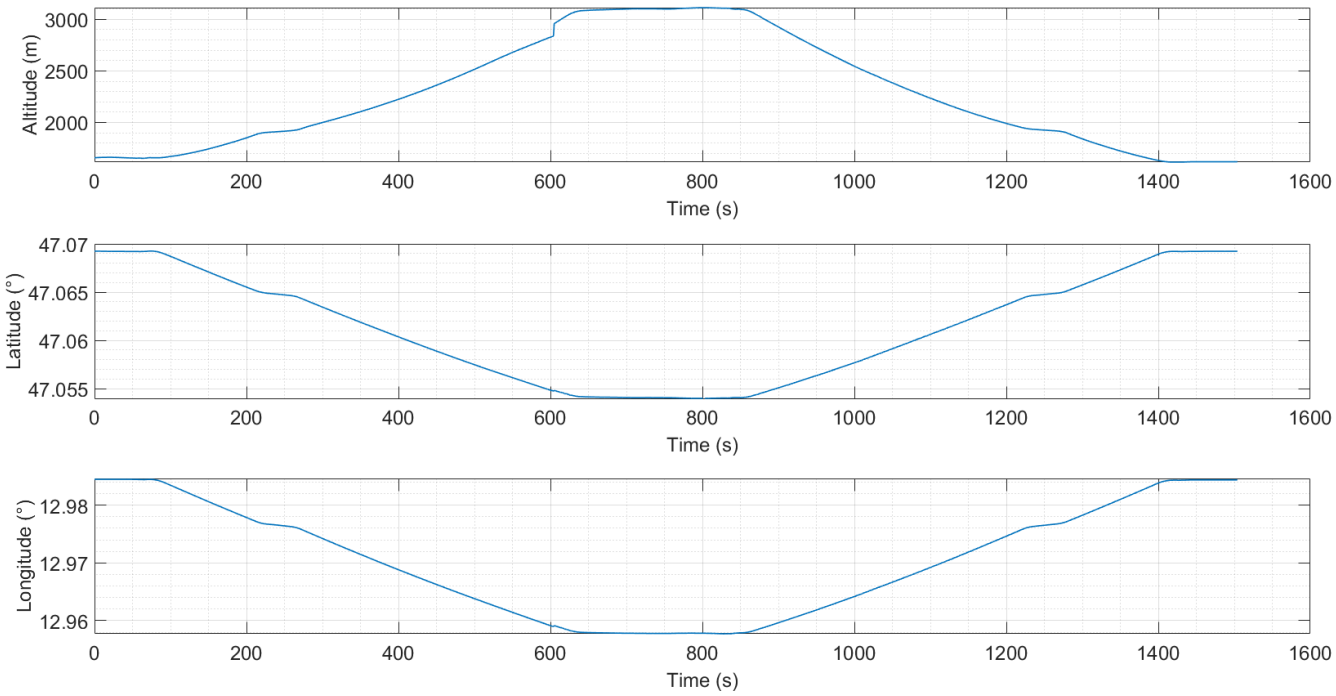

Fig. S3. GNSS data with lidar mounted horizontally

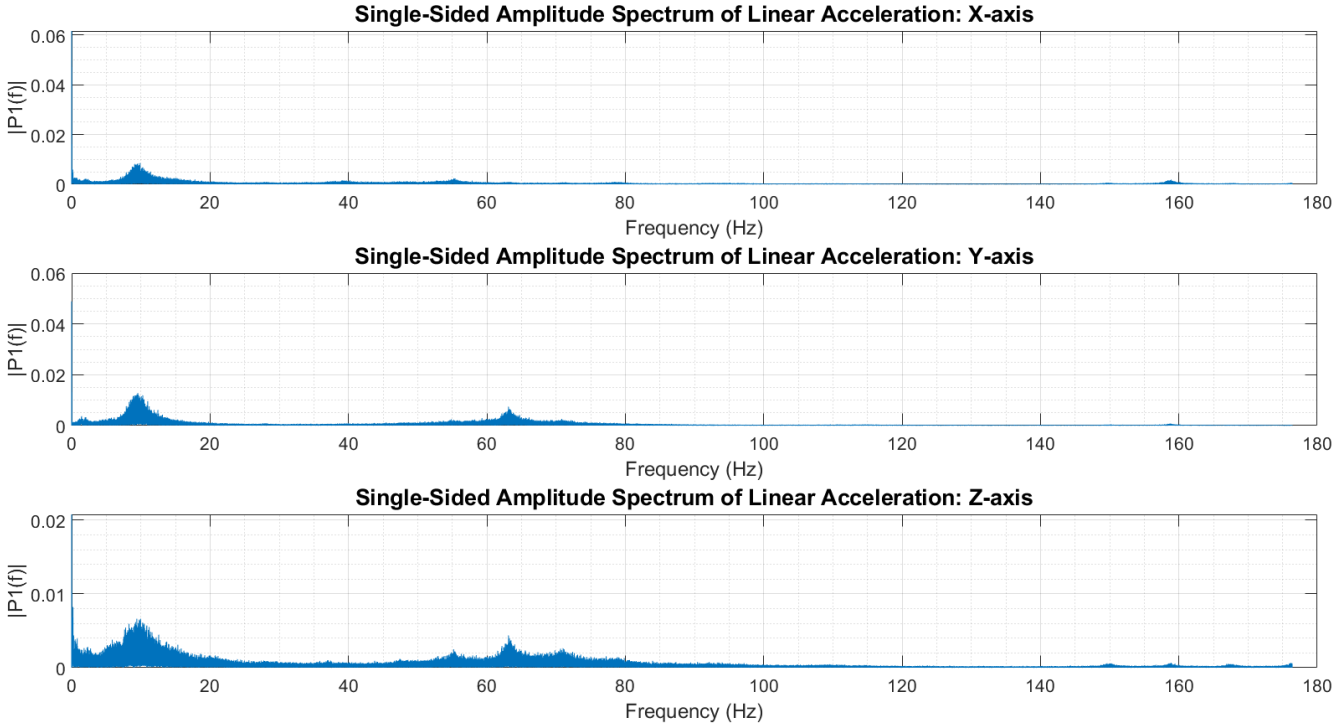

Fig. S4. FFT of the linear acceleration for the x-, y-, and z-axis with the lidar mounted horizontally

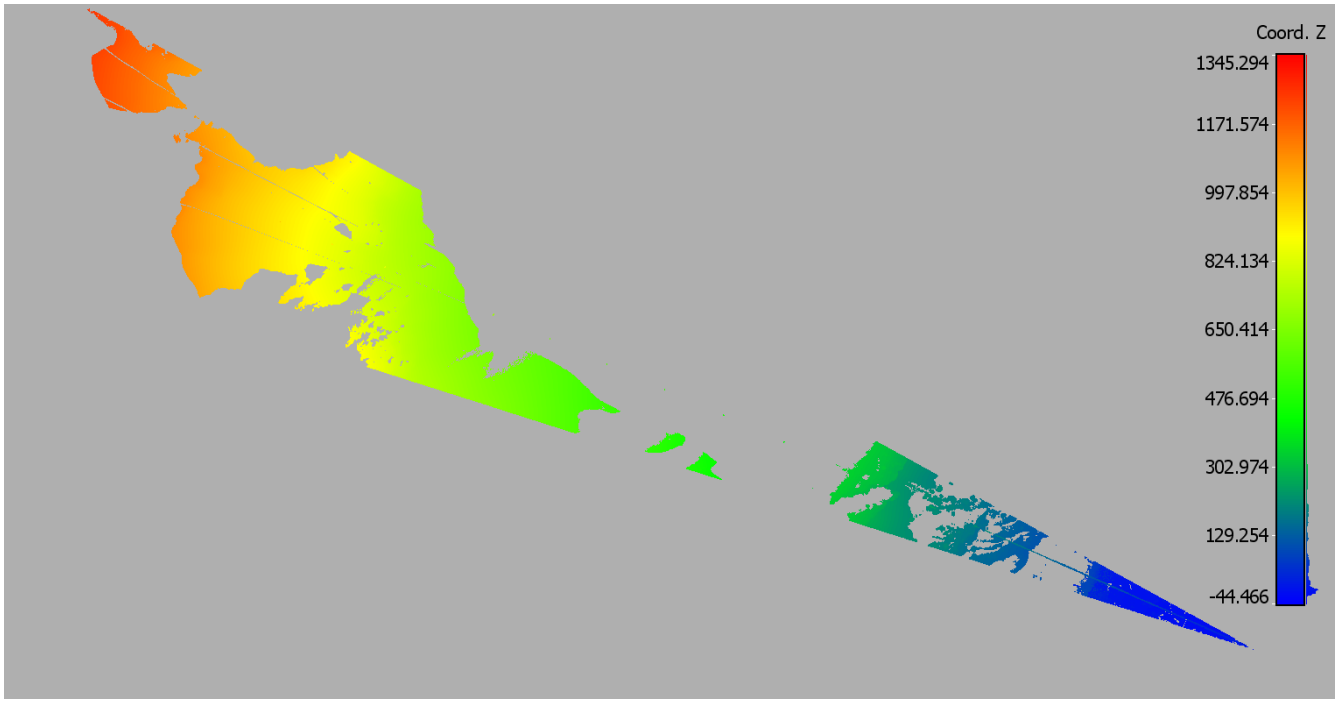

Fig. S5. Riegl VZ-6000 scan of the survey area showing large number of occluded areas

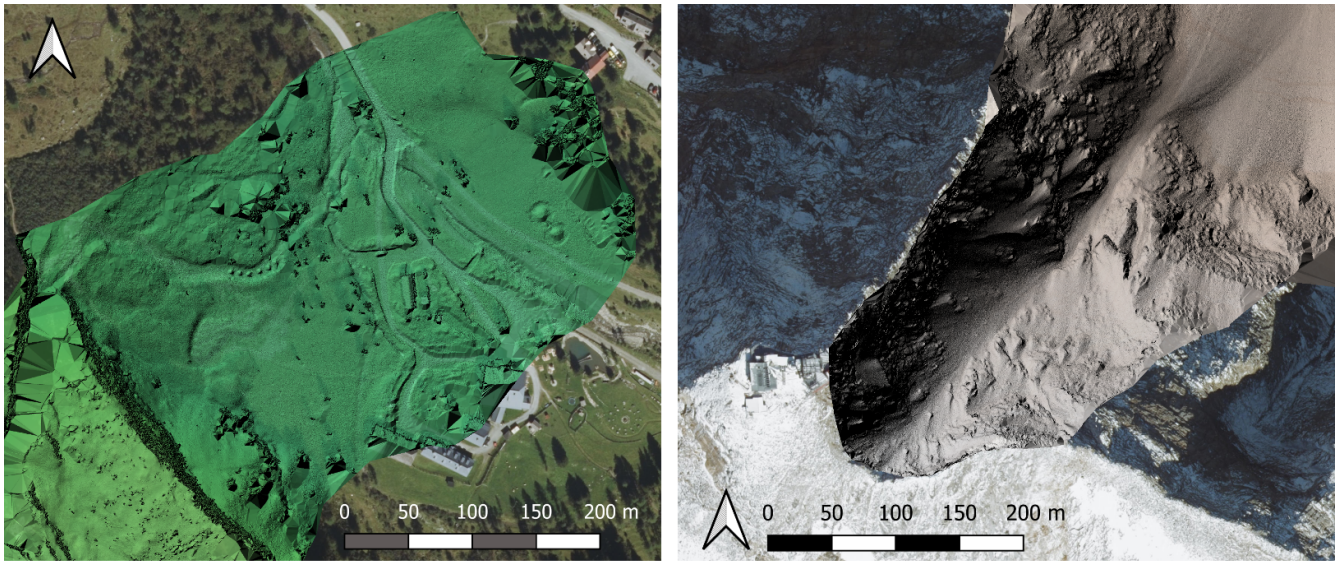

Fig. S6. 3D SLAM generated and subsequently georeferenced point cloud, with an aerial orthophoto from 2022 with 30 cm resolution from geolonad.at as a reference: (a) part near the valley station; (b) part near the mountain station